

Polyethylene Glycol/Rice Husk Ash Shape-Stabilized Phase Change Materials: Recovery of Thermal Energy Storage Efficacy via Engineering Porous Support Structure

Giang Tien Nguyen,* Bui Van Phuoc, Tran Thi Nhung, Le Thi Duy Hanh, Huynh Nguyen Anh Tuan, and Ly Tan Nhiem



Cite This: *ACS Omega* 2024, 9, 17104–17113



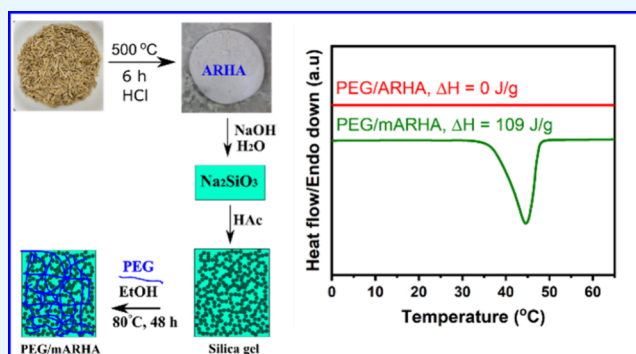
Read Online

ACCESS |

Metrics & More

Article Recommendations

ABSTRACT: This study focuses on modifying the porous structure of acid-treated rice husk ash (ARHA) to enhance the thermal energy storage capacity of poly(ethylene glycol) (PEG) confined within shape-stabilized phase change materials. The modification process involved a cost-effective sol–gel method in which ARHA was initially dissolved in an alkaline solution and subsequently precipitated in an acidic environment. ARHA, being a mesoporous SiO₂-based material with a high surface area but low pore volume, had limited capacity to adsorb PEG (50%). Furthermore, it hindered the crystallinity of impregnated PEG by fostering abundant interfacial hydrogen bonds (H-bonds), resulting in a diminished thermal energy storage efficiency. Following modification of the porous structure, the resulting material, termed mARHA, featured a three-dimensional macroporous network, providing ample space to stabilize a significant amount of PEG (70%) without any leakage. Notably, mARHA, with a reduced surface area, effectively mitigated interfacial H-bonds, consequently enhancing the crystallinity of impregnated PEG. This modification led to the recovery of thermal energy storage efficacy from 0 J/g for PEG/ARHA to 109.3 J/g for PEG/mARHA. Additionally, the PEG/mARHA composite displayed improved thermal conductivity, reliable thermal performance, and effective thermal management when used as construction materials. This work introduces a straightforward and economical strategy for revitalizing thermal energy storage in PEG composites confined within RHA-based porous supports, offering promising prospects for large-scale applications in building energy conservation.



1. INTRODUCTION

Shape-stabilized phase change materials (SSPCMs), which involve phase change materials enclosed within porous supports, have found widespread applications in building thermal management. This is attributed to their capability to enhance indoor temperature comfort and reduce energy consumption.^{1,2} Phase change materials (PCMs) function as thermal energy storage media, capable of absorbing, storing, and releasing latent heat during solid–liquid phase transition at a nearly constant temperature.³ Among various PCMs, polyethylene glycol (PEG) stands out for large-scale applications in buildings due to its cost-effectiveness, appropriate phase change temperature, and high cycle durability. Additionally, PEG exhibits characteristics such as low volume change, nontoxicity, high thermal energy storage capacity, and stability.^{4,5}

Simultaneously, porous supports serve to confine PCMs within nanopores, preventing potential leakage in liquid form through the capillary and surface tension forces.⁶ Various porous supports, including SiO₂, polymers, carbonaceous

materials, metal foams, and aerogels, are commonly employed for confining PCMs.^{6–8} Among these options, SiO₂ is widely favored for its tunable porous structure, high thermal stability, wide availability, and nontoxic nature.⁹ Furthermore, SiO₂ has demonstrated the capability to adsorb substantial amounts of PCMs, reaching up to 70–80%, thereby offering high thermal energy storage capacity for resulting SSPCMs.^{10,11} Notably, the SiO₂ prepared by Li et al.¹² achieved stabilization of up to 97% PEG, marking the highest PCM loading level reported. It is worth mentioning that in these investigations, chemical-grade tetraethyl orthosilicate (TEOS) was often employed as the SiO₂ precursor due to its convenience. However, the large-

Received: November 26, 2023

Revised: March 22, 2024

Accepted: March 25, 2024

Published: April 2, 2024



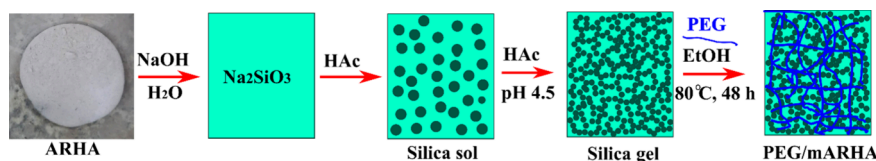


Figure 1. Preparation scheme of mARHA and the PEG/mARHA SSPCMs.

scale production of SSPCMs using TEOS faces challenges related to high cost and toxicity, posing limitations in thermal management applications. Additionally, the hydrolysis and condensation processes of TEOS are intricate, requiring precise control of reaction temperature, time, and pH values, leading to difficulties in controlling the resulting SiO_2 porosities and morphologies. Importantly, the low solubility of TEOS in water necessitates the addition of cosolvents, potentially impacting cost and environmental considerations.^{12–14} Therefore, there is a crucial need to develop a low-cost and environmentally friendly method for producing SiO_2 with desirable characteristics for integration with PCMs.

Rice stands out as a staple food globally, sustaining billions of people daily. The rice husk (RH), the protective layer enveloping rice grains, emerges as a significant byproduct postmilling, finding utility as biomass fuel in thermal power plants for heat provision. The combustion of RH gives rise to rice husk ash (RHA), deemed solid waste.¹⁵ Handling and utilizing the substantial volume of RHA pose challenges. Fortunately, RHA comprises only a small amount of oxide impurities and the rest is noncrystalline SiO_2 in finely particulate form, featuring numerous pores resulting from the aggregation of SiO_2 nanoparticles. This porous characteristic opens potential for serving as a porous support for stabilizing PCMs. Liu et al.¹⁶ employed HCl to treat RHA, removing a significant portion of impurities and yielding a mesoporous structure with a modest pore volume of $0.1783 \text{ cm}^3/\text{g}$. The treated RHA exhibited a loading level of 50% for a paraffin PCM. Yu et al.¹⁵ adopted a combination of HCl and ultrasonic treatment to eliminate impurities, revealing a mesoporous RHA structure with a pore volume of $0.1637 \text{ cm}^3/\text{g}$ and a PEG loading level of 62.1%. While acid treatment effectively eliminated impurities, resulting in relatively pure SiO_2 , the PCM loading levels of 50–62.1% for acid-treated RHA materials were notably lower compared to the 70–97% values achieved with TEOS-based synthesized SiO_2 , as mentioned earlier. The low mesopore volumes of 0.1637 – $0.1783 \text{ cm}^3/\text{g}$ in the porous structure of acid-treated RHA proved insufficient for adsorbing substantial amounts of PCMs. This diminished PCM loading typically translates to subpar thermal energy storage capacity, adversely impacting the overall thermal performance adversely. Consequently, a novel strategy for RHA treatment is imperative to enhance PCM loading further.

It is noted that hazardous wastes such as fly ash and oil shale ash have been recently investigated for the extraction of sodium silicate, which was further used as a SiO_2 precursor for the preparation of porous SiO_2 supporting for PEG-based SSPCMs.^{17,18} The obtained porous SiO_2 materials could exhibit high PEG adsorption of up to 80%, comparable to those synthesized from TEOS as mentioned earlier. These results suggested a promising strategy to enhance the PEG adsorption of RHA. With a high SiO_2 content, RHA could be a great source to produce high-quality sodium silicate for the preparation of porous SiO_2 . By this way, the original porous system of RHA could be turned into a more suitable structure

for high adsorption of PEG. However, to our best knowledge, there is a lack of studies reporting the use of RHA as a sodium silicate source to prepare a PEG/ SiO_2 SSPCM. It leads to a knowledge gap on the treatment and extraction of sodium silicate from RHA as well as the thermal performance of the novel PEG/ SiO_2 SSPCM compared to the original PEG/RHA SSPCM.

In this study, we first treated RHA with acid to remove impurities and then the obtained acid-treated RHA (ARHA) experienced structure modification for supporting PEG. The structure modification involved dissolving ARHA in an alkaline solution to obtain a sodium silicate solution and then reprecipitating it in an acidic condition, resulting in what we termed modified ARHA (mARHA). The modification process was straightforward and cost-effective, requiring only sodium hydroxide and acetic acid. We impregnated both ARHA and mARHA with varying amounts of poly(ethylene glycol) (PEG), leading to the formation of PEG/ARHA and PEG/mARHA SSPCMs. We extensively characterized and discussed the morphology, porosity, PEG adsorption capacity, and thermal energy storage performance of these SSPCMs. Our findings indicate that mARHA, with its favorable porous structure, significantly improves PEG adsorption and crystallinity compared to ARHA. Consequently, PEG/mARHA SSPCMs exhibit excellent thermal stability, thermal conductivity, and thermal reliability. Furthermore, we prepared construction materials incorporating PEG/mARHA SSPCMs with gypsum and investigated their effectiveness in building thermal management.

2. RESULTS AND DISCUSSION

2.1. Characterization. In this work, the porous structure of acid-treated RHA (ARHA) underwent modification through a sol–gel method to yield structure-modified ARHA (mARHA), as depicted in Figure 1. In this process, ARHA was first hydrolyzed in an alkaline environment to obtain a sodium silicate (Na_2SiO_3) solution. Upon adding acetic acid to the solution, silica sol was gradually formed and further polymerized into three-dimensional (3D) silica gel when the solution reached a pH value of 4.5.¹⁹ When PEG was added to the gel, it was adsorbed and dispersed in the 3D structure, forming PEG/mARHA SSPCMs.

The SEM images of ARHA are shown in Figure 2a,b, revealing irregular clumps (Figure 2a) with rough surfaces (Figure 2b). The N_2 adsorption–desorption isotherm of ARHA (Figure 3a) displayed a type IV isotherm indicative of a mesoporous structure. The mesopores exhibited sizes ranging from 2 to 20 nm, with peaks within 5–10 nm, as observed from the pore size distribution (PSD) curve (Figure 3b). ARHA exhibited a low pore volume of $0.28 \text{ cm}^3/\text{g}$ and a high specific surface area of $158 \text{ m}^2/\text{g}$, consistent with prior reports on its mesoporous structure and low pore volume.^{15,16} After the structural modification, the SEM images of mARHA (Figure 2c,d) revealed spherical particles of approximately 120–350 nm clustered into a highly interconnected porous

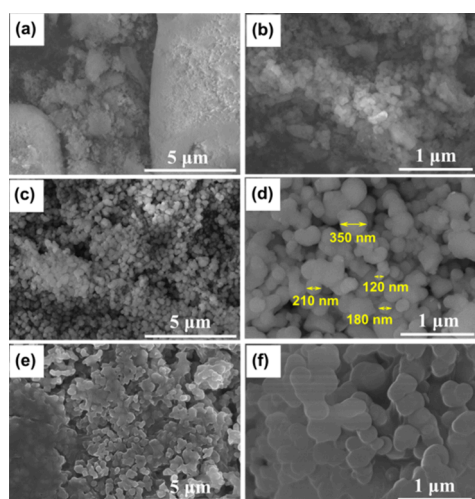


Figure 2. SEM images of (a, b) ARHA, (b, c) mARHA, and (e, f) 70% PEG/mARHA SSPCM.

structure with a significant proportion of macropores, facilitating PEG infiltration. The N_2 adsorption–desorption isotherm of mARHA (Figure 3a) exhibited a type II isotherm, typical for a macroporous material. The corresponding PSD of mARHA (Figure 3b) demonstrated the disappearance of most mesopores present in the original ARHA, resulting in a low specific surface area of $16 \text{ m}^2/\text{g}$ and a pore volume of $0.02 \text{ cm}^3/\text{g}$. These results indicated the successful modification of the mesoporous structure of ARHA into a macroporous structure in mARHA.

The PEG/mARHA SSPCMs were fabricated with varying PEG contents of 50, 60, 70, and 80%. SEM images of a representative sample at 70% PEG are presented in Figure 1e, f, illustrating the infiltration of PEG into the porous structure of mARHA and its adsorption on mARHA surfaces. Moreover, the corresponding N_2 adsorption and PSD curve (Figure 3a, b) indicated almost no N_2 adsorption and pores, affirming the successful impregnation of PEG into the mARHA porous network.

In addition to PEG/mARHA SSPCMs, PEG/ARHA SSPCMs were prepared with 50 and 60% PEG for the purpose of thermal efficacy comparison. Figure 4a compares the FTIR spectra of the prepared 50 and 60% PEG/ARHA SSPCMs to pure PEG and ARHA, while Figure 4b compares

the spectra of two representatives of 50 and 70% PEG/mARHA SSPCMs to pure PEG and mARHA. In the spectrum of pure PEG, characteristic absorption peaks of the C–H group were observed at 2888 , 1464 , 1294 , 956 , and 844 cm^{-1} , and the absorption peak of the C–O–C bond was situated at 1112 cm^{-1} . The peak at 3413 cm^{-1} was attributed to the absorption of the –OH group.²⁰ Both ARHA (Figure 4a) and mARHA (Figure 4b) exhibited characteristic peaks of siliceous material, with Si–O–Si vibrations observed at approximately 1100 , 810 , and 460 cm^{-1} . Additionally, peaks at approximately 3425 cm^{-1} were attributed to the overlapped absorption of silanol (Si–OH) groups on SiO_2 surfaces and adsorbed water.²¹ The patterns of both PEG/ARHA SSPCMs and PEG/mARHA SSPCMs incorporated the full characteristic peaks of PEG and their corresponding porous support without introducing new peaks, demonstrating physical interactions between PEG and the porous materials. It is noteworthy that the PEG chains, rich in oxygen elements and hydroxyl groups at the chain ends, would form interfacial hydrogen bonds (H–bonds) with the surface silanol groups on both ARHA and mARHA, as demonstrated in the literature.^{22–25}

2.2. Leakage Resistance of PEG/ARHA and PEG/mARHA SSPCMs. Figure 5 illustrates the leakage resistance of PEG/ARHA SSPCMs in comparison to PEG/mARHA SSPCMs after thermal treatment for 60 min at $60 \text{ }^\circ\text{C}$ ($\sim 20 \text{ }^\circ\text{C}$ above the melting point of PEG). For reference, pure PEG was included in the test and showed complete deformation due to melting (Figure 5). Notably, mARHA exhibited superior PEG adsorption capacity compared with ARHA. Specifically, ARHA could only accommodate and stabilize 50% of PEG, as evidenced by the leakage observed in the 60% PEG/ARHA composite. In contrast, mARHA effectively confined up to 70% PEG without any leakage in the PEG/mARHA SSPCMs with 50–70% PEG. This enhancement in PEG adsorption from 50% in ARHA to 70% in mARHA indicated an enriched PEG storage capacity, promising improved thermal performance. Comparatively, the 70% PEG stabilization of mARHA was higher than values of 50–62.1% of other RHA-based materials without structure modification in previous reports.^{15,16} The limited PEG adsorption of ARHA was attributed to its low mesoporous volume ($0.28 \text{ cm}^3/\text{g}$). Conversely, mARHA, with its macroporous structure, provided a substantial pore volume for efficient PEG storage. The interconnected porous network not only facilitated the storage of PEG but also established transport pathways for melted PEG. In the presence of

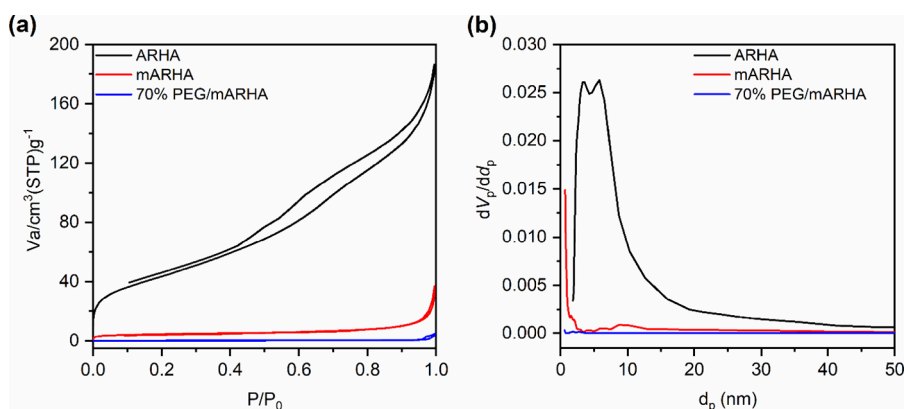


Figure 3. (a) N_2 adsorption–desorption isotherms of ARHA, mARHA, and the prepared 70% PEG/mARHA SSPCM, and (b) their relevant pore size distribution curves.

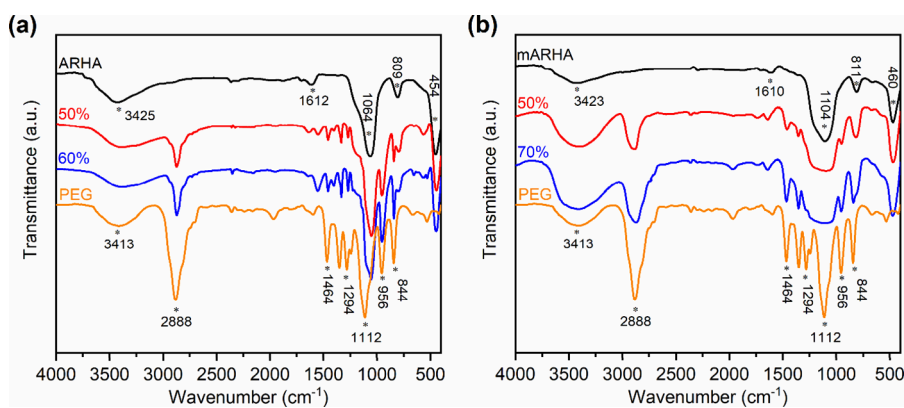


Figure 4. FTIR patterns of (a) ARHA, PEG, and the prepared PEG/ARHA SSPCMs at 50 and 60% PEG, and (b) mARHA, PEG, and the prepared PEG/mARHA SSPCMs at 50 and 70% PEG.

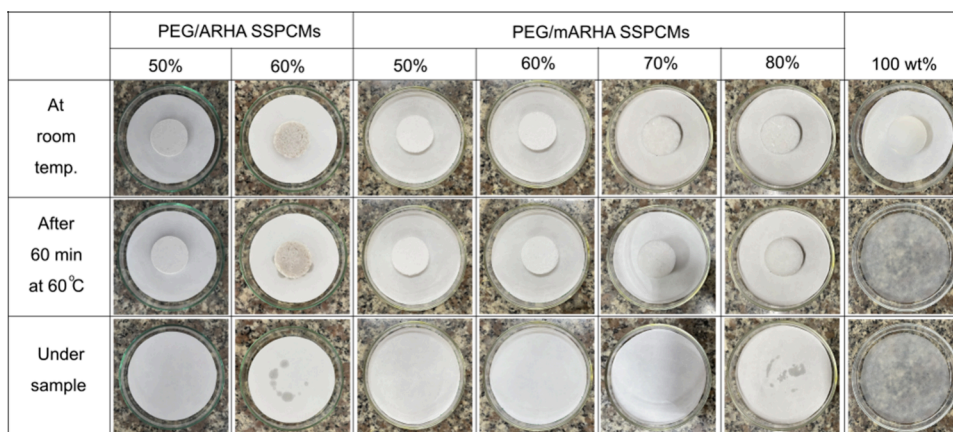


Figure 5. Digital photos of the PEG/ARHA SSPCMs and PEG/mARHA SSPCMs during the leakage–resistance test.

mARHA, PEG was stabilized through capillary action, surface tension, and interfacial hydrogen bonds, effectively preventing spillover of melted PEG from the mARHA porous network. It is important to note that 60% PEG/ARHA and 80% PEG/mARHA were excluded from subsequent characterization due to their inadequate leakage resistance.

2.3. Phase Change Properties of PEG/ARHA SSPCMs and PEG/mARHA SSPCMs. The phase change properties of PEG/ARHA and PEG/mARHA SSPCMs were thoroughly assessed and compared by using DSC measurements. Figure 6a,b displays the DSC curves of 50% PEG/ARHA and 50–70% PEG/mARHA SSPCMs. The crucial thermal parameters, including the melting/crystallization temperature (T_M/T_C) and melting/crystallization enthalpy ($\Delta H_M/\Delta H_C$), are summarized in Table 1. Notably, the 50% PEG/ARHA SSPCM exhibited no discernible signals of melting and crystallization in the DSC curves, indicative of a lack of heat storage capacity. The confinement within ARHA restricted the free mobility of PEG, disrupting the ordered arrangement necessary for crystallization due to interfacial hydrogen bonds (H-bonds).^{26,27} This suppression of the phase change enthalpy was further confirmed by the absence of crystalline peaks in the XRD pattern of 50% PEG/ARHA SSPCM (Figure 6c). Similar observations of suppressed crystallinity in mesoporous SiO₂-confined PEG have been reported in the literature.^{28,29} Due to its poor thermal efficiency, the PEG/ARHA SSPCM is not considered a viable material for thermal energy storage and will not be further explored.

The DSC curves of the prepared 50–70% PEG/mARHA composites exhibited distinct endothermic and exothermic peaks in the melting and crystallization curves, respectively, indicating their ability to conduct heat storage and release. The XRD patterns of representatives at 50 and 70% PEG (Figure 6c) displayed crystalline peaks at 2θ of 19.4 and 23.4°, precisely matching the crystal planes (120) and (032) of PEG.^{30,31} This confirmed the robust crystallization of confined PEG within the mARHA structure. In comparison to ARHA, which boasted a high surface area (158 m²/g), mARHA, with a substantially lower surface area (16 m²/g), engendered fewer interfacial hydrogen bonds between surface silanol groups and PEG. Consequently, the enhanced mobility of PEG within the mARHA structure facilitated the recovery of thermal energy storage in PEG/mARHA SSPCMs.

The PEG/mARHA SSPCMs exhibited single-phase transition processes with slightly reduced melting (T_M) and crystallization (T_C) temperatures compared to pure PEG (Table 1). The lower phase change temperatures indicated the presence of interfacial interactions, such as hydrogen bonds, capillary forces, and surface tension, between PEG and mARHA surfaces.^{17,19} The phenomenon was also observed in existing literature.^{21,32} The melting and crystallization enthalpies ($\Delta H_M/\Delta H_C$) of the PEG/mARHA SSPCMs, detailed in Table 1, increased with escalating PEG content, reaching 109.3 J/g at 70% PEG. This augmentation in enthalpy was attributed to the higher PEG content contributing to a larger quantity of absorbed/released thermal energy, as the

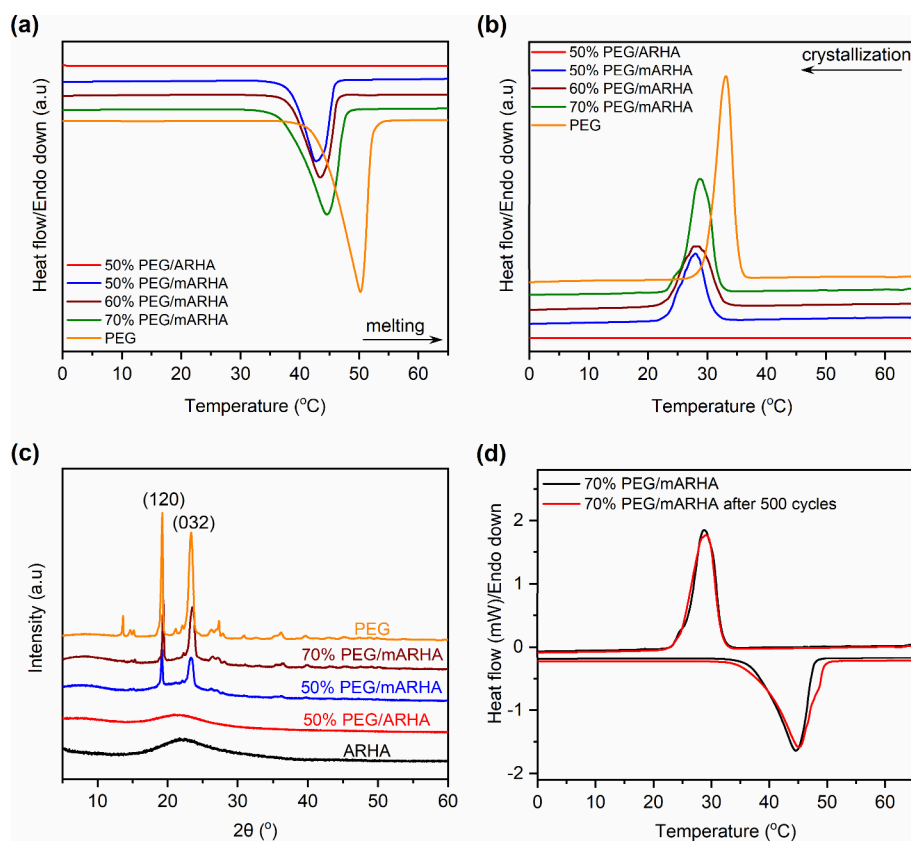


Figure 6. (a) Melting DSC thermograms of 50% PEG/ARHA SSPCM and 50–70% PEG/mARHA SSPCMs, (b) crystallization DSC thermograms of 50% PEG/ARHA SSPCM and 50–70% PEG/mARHA SSPCMs, (c) XRD spectra of PEG, mARHA, 50% PEG/ARHA SSPCM, and 50 and 70% PEG/mARHA SSPCMs, and (d) DSC curves of 70% PEG/mARHA before and after 500 thermal cycles.

Table 1. Phase Change Properties of 50% PEG/ARHA SSPCM and 50–70% PEG/mARHA SSPCMs

	T_M (°C)	ΔH_M (J/g)	T_C (°C)	ΔH_C (J/g)	F (%)
50% PEG/ARHA		0		0	0
50% PEG/mARHA	37.4	68.4	32.2	65.8	79.9
60% PEG/mARHA	37.6	88.6	32.8	86.5	86.3
70% PEG/mARHA	37.3	109.3	32.5	106.1	91.2
PEG	41.9	171.1	36.3	168.8	100
70% PEG/mARHA after 500 cycles	36.8	111.9	32.5	107.4	93.4

porous carrier played no role in phase change enthalpy. Additionally, the interactions between PEG and mARHA surface groups that initially suppressed PEG crystallinity appeared to be alleviated at higher PEG contents. The crystallinity of PEG confined in mARHA was estimated through its crystallization fraction ($F(\%)$), calculated using eq 1.²⁷

$$F = \frac{\Delta H_{\text{SSPCM}} \times 100}{\Delta H_{\text{PEG}} \times w} \quad (1)$$

where ΔH_{SSPCM} and ΔH_{PEG} are the melting enthalpies of PEG/mARHA SSPCMs and pure PEG, respectively, and w is the mass fraction of PEG in SSPCM. The resulting F values (Table 1) exhibited an increase from 79.9 to 91.2% with an elevation in PEG content from 50 to 70%. This indicates that the crystallinity of confined PEG was enhanced at higher PEG contents. As discussed earlier, in the SSPCM form, the

interaction of PEG with mARHA surfaces formed interfacial hydrogen bonds with surface silanol groups, leading to suppressed crystallinity. However, when the surfaces of mARHA were entirely covered with a layer of PEG, subsequent sublayers of PEG were not in contact with the surfaces and were excluded from interfacial hydrogen bonds. Consequently, an increase in the PEG content in SSPCMs enhanced the ratio of free PEG, leading to an improvement in crystallinity.

PEG confined in other mesoporous silica materials such as MCM-41 and SBA-15 also presented suppressed crystallinities (0–34%) due to H-bond interactions (Table 2). Surface modification of these materials with amino groups and polydopamine had been applied to reduce the interfacial interaction effects and recover thermal performance for confined PEG. Even so, the crystallinities of confined PEG were still significantly affected and gained values of only 50–80.7% (Table 2). Even more, the surface modification often required expensive reagents and relatively complicated reactions, challenging large-scale production and applications. In this work, the crystallinity of confined PEG was effectively recovered to 91.2% by modifying the mesoporous system of ARHA to a macroporous one of mARHA, using a simple and low-cost sol-gel method. Additionally, the thermal performance of the optimum 70% PEG/mARHA SSPCM was comparable to or even surpassed that of other PEG-based SSPCMs (Table 2). It showed better optimum PEG adsorption and crystallinity than PEG/Fe₃O₄-graphene/SiO₂ and PEG/Dop-SF. The PEG/Mica exhibited a slightly higher crystallinity (98.5%); however, its optimum PEG adsorption of

Table 2. Thermal Performance of PEG/mARHA SSPCM Compared with Reported PEG-Based SSPCMs

SSPCMs	optimum PEG adsorption (%)	ΔH_M (J/g)	F (%)	ref
PEG/ARHA	50	0	0	this work
PEG/mARHA	70	109.3	91.2	this work
PEG/SBA-15	70	0	0	29
PEG/amino-modified SBA-15	70	88.2	80.7	29
PEG/MCM-41	70	0	0	28
PEG/amino-modified MCM-41	60	58.76	64.0	28
PEG/SBA-15	70	47.25	34.0	33
PEG/polydopamine-modified SBA-15	70	69.77	50.0	33
PEG/Fe ₃ O ₄ -graphene/SiO ₂	65	111.69	85.0	34
PEG/mica	42.64	77.75	98.5	20
PEG/Dop-SF	70	73.8	54.7	24
PEG/TEOS-based SiO ₂	97	164.9	95.2	12
PEG/Sr ²⁺ -BaCO ₃	95	148.8	82.6	5

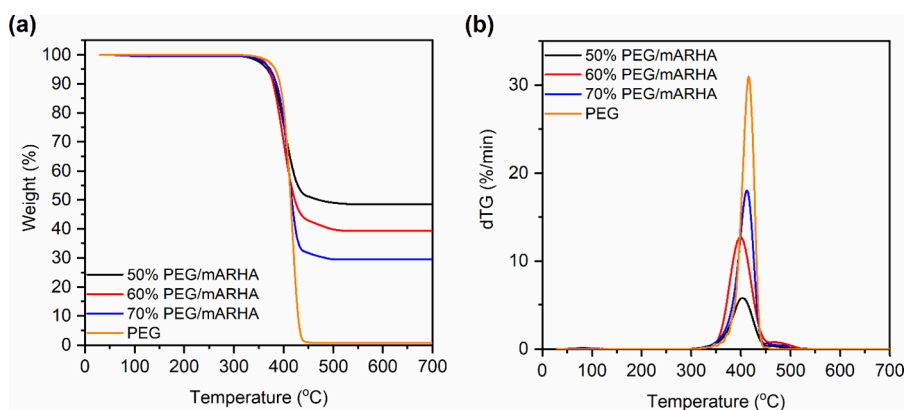
42.64% was much lower than the value of 70% of the PEG/mARHA. Although the PEG/Sr²⁺-BaCO₃- and PEG/TEOS-based SiO₂ presented impressive thermal performance compared to the prepared PEG/mARHA, the preparation of Sr²⁺-BaCO₃- and TEOS-based SiO₂ necessitated relatively expensive precursors and strictly controlled reactions. Overall, the simple preparation, high thermal performance, and cost-effectiveness make the PEG/mARHA promising for large-scale industrial applications.

The thermal reliability, often termed cycling durability, of the 70% PEG/mARHA SSPCM was rigorously examined through 500 phase change cycles. The results, as illustrated in Figure 6d, provide valuable insights into the stability and robustness of the composite. The DSC curve of the SSPCM after 500 accelerated thermal cycles closely resembled the original curve, as depicted in Figure 5d. The negligible changes in both melting (T_M) and crystallization (T_C) temperatures—0.5 and 0 °C, respectively—highlight the sustained thermal stability of the cyclic SSPCM. Most notably, the thermal energy storage capacity remained consistent after multiple thermal cycles. The differences in ΔH_M and ΔH_C before and after cycles were merely 3.3 and 1.2%, respectively, underscoring the composite's ability to maintain its thermal

performance over extended usage. The observed outcomes affirm the commendable thermal reliability of PEG/mARHA SSPCMs, positioning them as viable candidates for prolonged and consistent utilization in various thermal management applications.

2.4. Thermal Stability Analysis. The thermal stability of PEG/mARHA SSPCMs was assessed through TGA, and the corresponding TGA and DTG (derivative thermogravimetry) curves are illustrated in Figure 7. Pure PEG exhibited thermal decomposition in a one-step model within the temperature range of 376–440 °C, resulting in a weight loss of nearly 100%. Similarly, all the prepared SSPCMs underwent thermal decomposition in a one-step model, albeit with slightly lower decomposition temperature ranges compared to pure PEG. The DTG curves revealed that pure PEG had a T_{MAX} (temperature at a maximum decomposition rate) of 417 °C, while the SSPCMs displayed slightly lower T_{MAX} values ranging from 404 to 410 °C. The reduced thermal decomposition temperatures of the SSPCMs could be attributed to weaker physical interactions between PEG and mARHA compared to the intermolecular interactions among pure PEG molecules.¹² Importantly, the thermal decomposition temperatures of PEG/mARHA SSPCMs remained considerably higher than the Earth's surface temperature, indicating excellent thermal stability for applications in building thermal management. Furthermore, the practical PEG contents, determined from the TGA curves, closely matched the targeted contents of 50, 60, and 70%, confirming the even dispersion of PEG within the mARHA structure.

2.5. Thermal Conductivity Analysis. The thermal conductivities of PEG/mARHA SSPCMs were evaluated and compared to pure PEG, with the results depicted in Figure 8. Pure PEG exhibited a suboptimal thermal conductivity of 0.28 W/(m · K), representing a significant drawback that hinders the rate of heat transfer during thermal storage and release. However, in the form of SSPCMs, the thermal conductivities showed a marked improvement, increasing by 2.03–1.43 times to 0.61–0.40 W/m·K with an increase in PEG content from 50 to 70%, respectively. This enhancement in thermal conductivity can be attributed to the incorporation of the siliceous support, which possesses relatively high thermal conduction characteristics. Furthermore, the three-dimensional porous structure of mARHA contributes to an increased surface area for PEG, providing an effective thermally conductive scaffold that establishes a thermal pathway, thereby enhancing thermal conductivity.^{35,36} The observed increase in thermal con-

**Figure 7.** (a) TGA curves of PEG and the PEG/mARHA SSPCMs and (b) the relevant DTG curves.

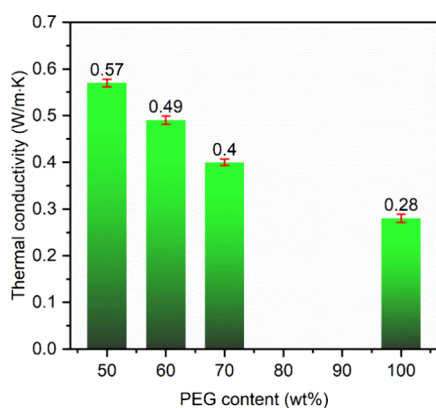


Figure 8. Thermal conductivities of PEG and prepared PEG/mARHA SSPCMs.

ductivity with rising mARHA content in SSPCMs aligns with previous findings demonstrating that SiO₂-based SSPCMs with PCM contents ranging from 50 to 80% exhibited a 1.33–2.01 times improvement in thermal conductivity compared to that of pure PCMs.^{10,19} This heightened thermal conductivity is advantageous for enhancing the thermal storage and release performance of the PEG/mARHA SSPCMs.

2.6. Heat Transfer Retardation in Construction Material. To showcase the effectiveness of PEG/mARHA SSPCMs in building thermal management, a composite containing 70% PEG/mARHA was integrated with gypsum at SSPCM contents of 15 and 30%. Figure 9 offers a

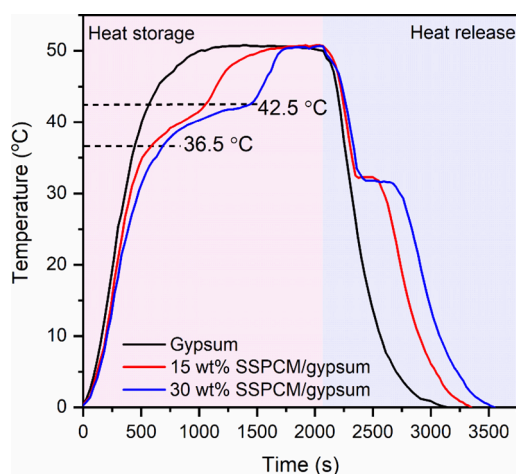


Figure 9. Temperature–time curves of PEG/mARHA SSPCM/gypsum mixtures compared to pristine gypsum.

comparative analysis of temperature–time curves for bare gypsum and SSPCM-combined gypsums during the heating and cooling phases within the temperature range 0–55 °C. During the heating phase, the temperature of SSPCM-combined gypsums initially experienced a rapid increase

attributed to sensible heat absorption. Upon reaching approximately 36.5 °C, the temperature rise rate markedly decelerated, leading to temperature plateaus until around 42.5 °C. This phenomenon was a result of PEG melting in the SSPCM, driven by both sensible and latent heat absorption. Subsequently, the temperature resumed a rapid increase due to sensible heat adsorption. In contrast, bare gypsum exhibited a swift temperature rise throughout the entire heating process, lacking latent heat storage capability. For instance, to reach 42.5 °C, bare gypsum required only 570 s while the 15% SSPCM/gypsum and 30% SSPCM/gypsum needed up to 1050 and 1440 s, respectively. These findings highlight that the incorporation of SSPCMs into gypsum can significantly impede heat transfer into buildings, thereby contributing to energy savings.

3. CONCLUSIONS

In summary, this study successfully enhanced the heat storage performance of PEG/mARHA SSPCMs compared to that of PEG/ARHA SSPCMs by modifying the porous structure of ARHA using a straightforward sol–gel method. ARHA exhibited a mesoporous structure with a low pore volume (0.28 cm³/g), leading to poor PEG adsorption (only 50%). The high surface area of ARHA (158 m²/g) facilitated interfacial H–bonds with PEG, suppressing the crystallinity of confined PEG and resulting in reduced thermal energy storage. The mARHA provided sufficient pore volume to adsorb up to 70% PEG without leakage due to its macroporous structure. The low surface area of mARHA (16 m²/g) promoted the crystallinity of confined PEG by reducing the number of interfacial H–bonds. A high thermal energy storage capacity (109.3 J/g) was achieved for 70% PEG/mARHA, compared to 0 J/g for PEG/ARHA. 70% PEG/mARHA demonstrated a 1.42 times increase in thermal conductivity compared to pure PEG. It exhibited high thermal stability, durability after 500 melting/crystallization cycles, and effective performance in building thermal management. With these promising properties and simple preparation, 70% PEG/mARHA could not only serve as a low-cost material for building energy savings, showcasing its potential as an efficient solution in the realm of construction and thermal management but also significantly contribute to the treatment and raise value for RHA.

4. MATERIALS AND METHODS

4.1. Materials. Rice husk was obtained from a local shop in Ho Chi Minh City, Vietnam. PEG (molecular weight 1000), absolute ethanol, sodium hydroxide, and glacial acetic acid were obtained from Shanghai Zhanyun Chemical (China).

4.2. Preparation of ARHA. The preparation of ARHA is illustrated in Figure 10. RH was calcined at 600 °C in a muffle furnace for 6 h to obtain RHA (RHA). The as-obtained RHA was treated for removing impurities by refluxing with a 2 M HCl solution for 4 h. Then, it was filtered under low pressure

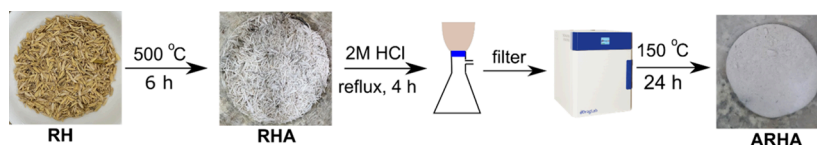


Figure 10. Preparation scheme of ARHA.

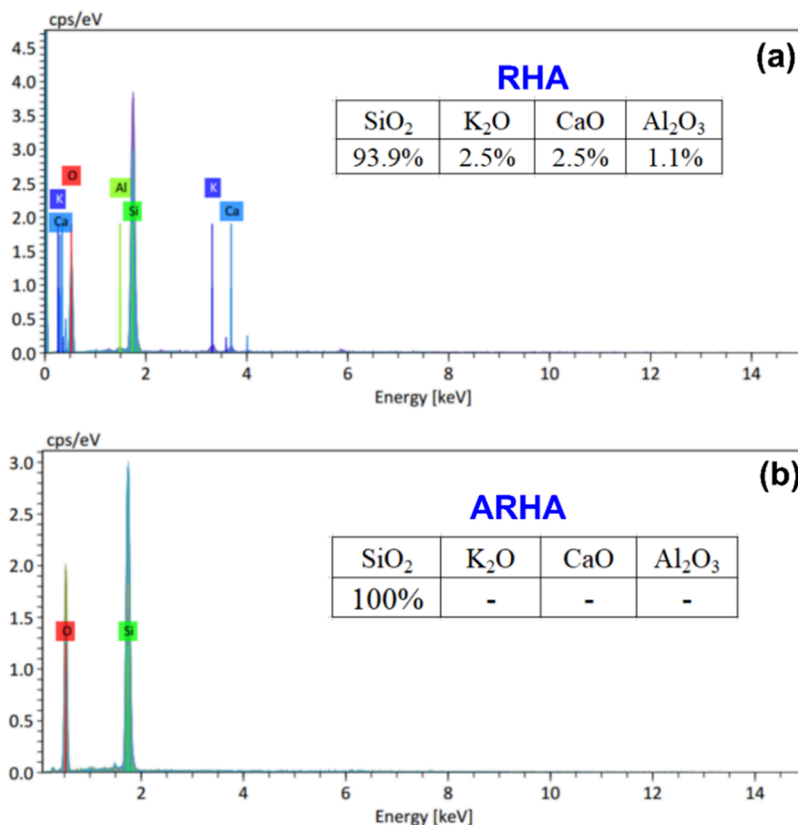


Figure 11. EDS results and elemental compositions of (a) RHA and (b) ARHA.

and washed with distilled water until pH reached 6–7 and dried at 150 °C for 24 h, resulting in ARHA. The elemental compositions of RHA and ARHA were analyzed by the EDS method, and the results are shown in Figure 11. The RHA contained a small proportion of metallic oxide impurities, including Al₂O₃, K₂O, and CaO and up to 93.9% of SiO₂. After the treatment with HCl, the obtained ARHA was composed of almost 100% SiO₂ as no impurities were detectable by the EDS method.

4.3. Preparation of PEG/ARHA SSPCMs. PEG/ARHA SSPCMs were synthesized with PEG contents of 50 and 60% using an established method.^{27,29} PEG and ARHA in specified amounts were combined in ethanol and stirred at room temperature for 2 h. The mixture temperature was then elevated to 80 °C to facilitate solvent evaporation. The resultant products were subsequently dried in an oven at 80 °C for 12 h to ensure complete removal of ethanol, yielding PEG/ARHA SSPCMs.

4.4. Preparation of mARHA and PEG/mARHA SSPCMs. The mARHA and PEG/mARHA SSPCMs were prepared through a one-step procedure, as illustrated in Figure 12. Initially, 1.0 g of ARHA was dissolved in 20 mL of 4 M NaOH under magnetic stirring until a clear solution, containing some carbon impurities, was obtained. The carbon impurities were separated from the solution through vacuum filtration to collect a sodium silicate solution. Subsequently, 4 M CH₃COOH was added dropwise into the solution under magnetic stirring. When the pH value reached approximately 4.5, the solution was stirred for an additional 1 h, and then filtered, and washed four times with distilled water to collect a white product. PEG/mARHA SSPCMs were prepared by adding about 2–3 mL of ethanol and varying amounts of PEG

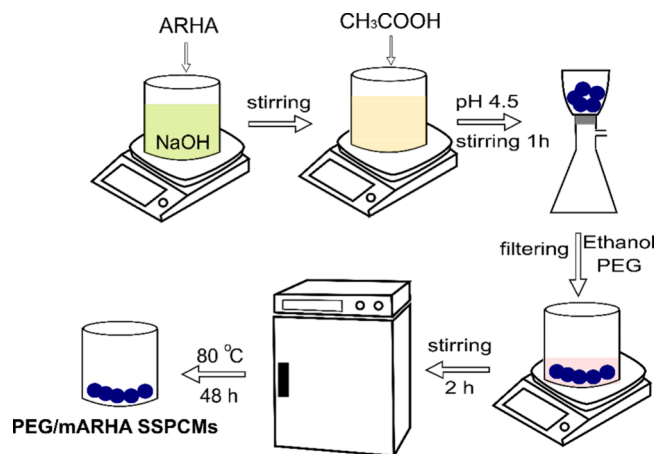


Figure 12. Illustration of the preparation process of mARHA and PEG/mARHA SSPCMs.

into the white product. The mixtures were stirred for 2 h and then dried in an oven at 80 °C for 48 h, yielding PEG/mARHA SSPCMs with increasing PEG contents (50, 60, 70, and 80%). To obtain a representative mARHA for characterization, the prepared 70% PEG/mARHA SSPCM was calcined at 500 °C for 6 h to remove PEG, leaving bare mARHA.

4.5. Characterization Methods. The elemental compositions were determined by using energy-dispersive X-ray spectroscopy (EDS) with a Hitachi TM4000 analyzer. Morphological properties were investigated through scanning electron microscopy (SEM) analysis using Hitachi S4800 equipment. N₂ adsorption–desorption isotherms were measured at the temperature of liquid N₂ (−196 °C) with

Micromeritics, MicroActive TriStar II Plus equipment. Specific surface areas were determined using the Brunauer–Emmett–Teller (BET) model, and PSDs were analyzed based on the nonlocal density functional theory (NLDFT).

Chemical structural determination was conducted by Fourier-transformed infrared spectroscopy (FT-IR) using a JASCO FTIR 4600 equipment at wavelengths ranging from 400 to 4000 cm^{-1} . Crystallization was studied using an Malvern Empyrean Powder X-ray diffractometer at 2θ of 5–50°. Phase change temperatures and enthalpies were analyzed by differential scanning calorimetry (DSC, 214 Polyma, Netzsch) under a N_2 atmosphere in a temperature interval of 0–65 °C, with a heating/cooling speed of 5 °C/min. Thermal stability was examined through thermogravimetric analysis (TGA) using Setaram LABSYS Evo TG-DSC 1600 equipment, measuring from room temperature to 700 °C at a heating speed of 10 °C/min under a N_2 atmosphere. Thermal conductivity was analyzed using the transient plane source method with a Hot Disk AB, TPS 3500 equipment.

Leakage resistance was tested by placing materials on filtered papers and subjecting them to thermal treatment for 60 min at 60 °C in an oven. Subsequently, filter papers were removed and materials were carefully observed for spots of PEG leakage. The cycling durability test involved 500 solid/liquid phase transition cycles, with approximately 1 g of material repeatedly solidifying and melting in lower-temperature (10 °C) and higher-temperature (55 °C) baths, each for 5 min.

For the application of PEG/mARHA SSPCM in building thermal management, the SSPCM with 70% PEG was mechanically mixed with gypsum at 15 and 30% SSPCM and their thermal transfer delay was evaluated compared to pristine gypsum using an apparatus developed in our recent report.³⁷ Briefly, a portion of 30 g of the tested material was packed in a cylinder (30 mm \times 70 mm), preconditioned in a lower-temperature bath (10 °C), and then moved to a higher-temperature bath (55 °C) for melting. After reaching plateau temperatures, the cylinder was moved back to the lower-temperature bath for crystallization. The temperature variation of the material was recorded with a thermocouple (Ika ETS-D5).

AUTHOR INFORMATION

Corresponding Author

Giang Tien Nguyen – Faculty of Chemical and Food Technology, Ho Chi Minh City University of Technology and Education (HCMUTE), Ho Chi Minh City 700000, Vietnam; orcid.org/0000-0003-0216-2735; Email: ntgiang@hcmute.edu.vn

Authors

Bui Van Phuoc – Faculty of Chemical and Food Technology, Ho Chi Minh City University of Technology and Education (HCMUTE), Ho Chi Minh City 700000, Vietnam

Tran Thi Nhung – Faculty of Chemical and Food Technology, Ho Chi Minh City University of Technology and Education (HCMUTE), Ho Chi Minh City 700000, Vietnam

Le Thi Duy Hanh – Faculty of Chemical and Food Technology, Ho Chi Minh City University of Technology and Education (HCMUTE), Ho Chi Minh City 700000, Vietnam

Huynh Nguyen Anh Tuan – Faculty of Chemical and Food Technology, Ho Chi Minh City University of Technology and

Education (HCMUTE), Ho Chi Minh City 700000, Vietnam

Ly Tan Nhiem – Faculty of Chemical and Food Technology, Ho Chi Minh City University of Technology and Education (HCMUTE), Ho Chi Minh City 700000, Vietnam; orcid.org/0000-0003-4775-6174

Complete contact information is available at: <https://pubs.acs.org/10.1021/acsomega.3c09417>

Notes

The authors declare no competing financial interest.

ACKNOWLEDGMENTS

This research is supported by the Ho Chi Minh City University of Technology and Education, Vietnam.

NOMENCLATURE

PEG	polyethylene glycol
RH	rice husk
RHA	rice husk ash
ARHA	acid-treated rice husk ash
mARHA	structure-modified acid-treated rice husk ash
PCM	phase change material
SSPCM	shape-stabilized phase change material
TEOS	tetraethyl orthosilicate
SEM	scanning electron microscope
BET	Brunauer–Emmett–Teller
NLDFT	nonlocal density functional theory
PSD	pore size distribution
FTIR	Fourier-transformed infrared spectroscopy
XRD	X-ray diffraction
DSC	differential scanning calorimetry
TGA	thermogravimetric analysis
T_M	melting temperature
T_C	crystallization temperature
ΔH_M	melting enthalpy
ΔH_C	crystallization enthalpy
F	crystallization fraction

REFERENCES

- Rathore, P. K. S.; Shukla, S. K. Enhanced thermophysical properties of organic PCM through shape stabilization for thermal energy storage in buildings: A state of the art review. *Energy Build.* **2021**, *236*, No. 110799.
- Lamrani, B.; Johannes, K.; Kuznik, F. Phase change materials integrated into building walls: An updated review. *Renewable Sustainable Energy Rev.* **2021**, *140*, No. 110751.
- Li, Z.-R.; Hu, N.; Fan, L.-W. Nanocomposite phase change materials for high-performance thermal energy storage: A critical review. *Energy Stor. Mater.* **2023**, *55*, 727–753.
- Sarcinella, A.; Barroso de Aguiar, J. L.; Jesus, C.; Frigione, M. Thermal properties of PEG-based form-stable Phase Change Materials (PCMs) incorporated in mortars for energy efficiency of buildings. *J. Energy Storage* **2023**, *67*, No. 107545.
- Mohaisen, K. O.; Zahir, M. H.; Maslehuddin, M. Shape-stabilized phase change material for thermal energy storage: Sr⁺² doped BaCO₃ matrix incorporating polyethylene glycol. *J. Energy Storage* **2023**, *58*, No. 106369.
- Li, Z.-R.; Hu, N.; Fan, L.-W. Nanocomposite phase change materials for high-performance thermal energy storage: A critical review. *Energy Storage Mater.* **2022**, *727* DOI: [10.1016/j.ensm.2022.12.037](https://doi.org/10.1016/j.ensm.2022.12.037).

- (7) Mishra, R. K.; Verma, K.; Mishra, V.; Chaudhary, B. A review on carbon-based phase change materials for thermal energy storage. *J. Energy Storage* **2022**, *50*, No. 104166.
- (8) Saqib, M.; Andrzejczyk, R. A review of phase change materials and heat enhancement methodologies. *Wiley Interdiscip. Rev. Energy Environ* **2023**, *12* (3), No. e467.
- (9) Tuan, H. N. A.; Tam, L. M.; Tien Nguyen, G. Methylated mesoporous silica loaded with 1-octadecanol as a new shape-stabilized phase change material for enhanced thermal energy storage efficiency. *Can. J. Chem.* **2023**, *101* (4), 235–241.
- (10) Qian, T.; Li, J.; Min, X.; Fan, B. Integration of Pore Confinement and Hydrogen-Bond Influence on the Crystallization Behavior of C18 PCMs in Mesoporous Silica for Form-Stable Phase Change Materials. *ACS Sustainable Chem. Eng.* **2018**, *6* (1), 897–908.
- (11) Min, X.; Fang, M.; Huang, Z.; Liu, Y.; Huang, Y.; Wen, R.; Qian, T.; Wu, X. Enhanced thermal properties of novel shape-stabilized PEG composite phase change materials with radial mesoporous silica sphere for thermal energy storage. *Sci. Rep.* **2015**, *5*, 12964.
- (12) Li, B.; Shu, D.; Wang, R.; Zhai, L.; Chai, Y.; Lan, Y.; Cao, H.; Zou, C. Polyethylene glycol/silica (PEG@SiO₂) composite inspired by the synthesis of mesoporous materials as shape-stabilized phase change material for energy storage. *Renew. Energy* **2020**, *145*, 84–92.
- (13) Nguyen, T. T. H.; Fukaya, N.; Sato, K.; Choi, J. C.; Kataoka, S. Design and assessment of an energy self-supply process producing tetraethyl orthosilicate using rice husk. *Bioresour. Technol.* **2022**, *344*, No. 126188.
- (14) Sharma, P.; Prakash, J.; Kaushal, R. An insight into the green synthesis of SiO₂ nanostructures as a novel adsorbent for removal of toxic water pollutants. *Environ. Res.* **2022**, *212*, No. 113328.
- (15) Yu, K.; Liu, Y.; Yang, Y. Enhanced thermal properties of polyethylene glycol/modified rice husk ash eco-friendly form-stable phase change material via optimizing support pore structure. *J. Energy Storage* **2021**, *43*, No. 103172.
- (16) Liu, Y.; Yu, K.; Lu, S.; Wang, C.; Li, X.; Yang, Y. Experimental research on an environment-friendly form-stable phase change material incorporating modified rice husk ash for thermal energy storage. *J. Energy Storage* **2020**, *31*, No. 101599.
- (17) Feng, L.; Yu, R.; Li, Y.; Huang, Y.; Zhao, L. Shape-stabilized phase change materials composed of polyethylene glycol and ordered mesoporous silica synthesized from fly ash. *Thermochim. Acta* **2023**, *720*, No. 179428.
- (18) Qian, T.; Li, J.; Ma, H.; Yang, J. The preparation of a green shape-stabilized composite phase change material of polyethylene glycol/SiO₂ with enhanced thermal performance based on oil shale ash via temperature-assisted sol-gel method. *Sol. Energy Mater. Sol. Cells* **2015**, *132*, 29–39.
- (19) Sun, K.; Kou, Y.; Zheng, H.; Liu, X.; Tan, Z.; Shi, Q. Using silicagel industrial wastes to synthesize polyethylene glycol/silica-hydroxyl form-stable phase change materials for thermal energy storage applications. *Sol. Energy Mater. Sol. Cells* **2018**, *178*, 139–145.
- (20) Zhang, D.; Li, C.; Lin, N.; Xie, B.; Chen, J. Mica-stabilized polyethylene glycol composite phase change materials for thermal energy storage. *Int. J. Miner. Metall.* **2022**, *29* (1), 168–176.
- (21) Nguyen, G. T.; Hwang, H. S.; Park, I. Effects of functional groups and alkyl chain lengths on non-freezable layer thickness of shape-stabilized phase change materials confined in mesoporous silica. *Int. J. Energy Res.* **2022**, *46* (9), 12687–12701.
- (22) Qi, G.-Q.; Liang, C.-L.; Bao, R.-Y.; Liu, Z.-Y.; Yang, W.; Xie, B.-H.; Yang, M.-B. Polyethylene glycol based shape-stabilized phase change material for thermal energy storage with ultra-low content of graphene oxide. *Sol. Energy Mater. Sol. Cells* **2014**, *123*, 171–177.
- (23) Zhang, S.; Tao, Q.; Wang, Z.; Zhang, Z. Controlled heat release of new thermal storage materials: the case of polyethylene glycol intercalated into graphene oxide paper. *J. Mater. Chem.* **2012**, *22* (38), 20166–20169.
- (24) Chen, Y.; Ding, H.; Wang, B.; Shi, Q.; Gao, J.; Cui, Z.; Wan, Y. Dopamine functionalization for improving crystallization behaviour of polyethylene glycol in shape-stable phase change material with silica fume as the matrix. *J. Cleaner Prod.* **2019**, *208*, 951–959.
- (25) Feng, L.; Zhao, W.; Zheng, J.; Frisco, S.; Song, P.; Li, X. The shape-stabilized phase change materials composed of polyethylene glycol and various mesoporous matrices (AC, SBA-15 and MCM-41). *Sol. Energy Mater. Sol. Cells* **2011**, *95* (12), 3550–3556.
- (26) Aftab, W.; Huang, X.; Wu, W.; Liang, Z.; Mahmood, A.; Zou, R. Nanoconfined phase change materials for thermal energy applications. *Energy Environ. Sci.* **2018**, *11* (6), 1392–1424.
- (27) Gao, H.; Wang, J.; Chen, X.; Wang, G.; Huang, X.; Li, A.; Dong, W. Nanoconfinement effects on thermal properties of nanoporous shape-stabilized composite PCMs: A review. *Nano Energy* **2018**, *53*, 769–797.
- (28) Feng, D.; Feng, Y.; Li, P.; Zang, Y.; Wang, C.; Zhang, X. Modified mesoporous silica filled with PEG as a shape-stabilized phase change materials for improved thermal energy storage performance. *Microporous Mesoporous Mater.* **2020**, *292*, No. 109756.
- (29) Wang, J.; Yang, M.; Lu, Y.; Jin, Z.; Tan, L.; Gao, H.; Fan, S.; Dong, W.; Wang, G. Surface functionalization engineering driven crystallization behavior of polyethylene glycol confined in mesoporous silica for shape-stabilized phase change materials. *Nano Energy* **2016**, *19*, 78–87.
- (30) Wu, Y.; Li, L.; Chen, S.; Qin, J.; Chen, X.; Zhou, D.; Wu, H. Synthesis, characterization, and crystallization behaviors of poly(D-lactic acid)-based triblock copolymer. *Sci. Rep.* **2020**, *10* (1), 3627.
- (31) Li, R.; Wu, Y.; Bai, Z.; Guo, J.; Chen, X. Effect of molecular weight of polyethylene glycol on crystallization behaviors, thermal properties and tensile performance of polylactic acid stereocomplexes. *RSC Adv.* **2020**, *10* (69), 42120–42127.
- (32) Nguyen, G. T.; Do, M. H.; Ly, T. N.; Park, I.; Bui, T. H. Novel shape-stabilized phase change materials: Insights into the thermal energy storage of 1-octadecanol/fumed silica composites. *J. Energy Storage* **2022**, *52*, No. 104772.
- (33) Gao, J.; Zhou, J.; Zhang, X.; Shi, Q.; Han, Z.; Chen, Y. Facile functionalized mesoporous silica using biomimetic method as new matrix for preparation of shape-stabilized phase-change material with improved enthalpy. *Int. J. Energy Res.* **2019**, *43* (14), 8649–8659.
- (34) Jannah, N. N.; Taufiq, A.; Zulaikah, S.; Hidayat, A.; Suharyadi, E.; Wicaksono, S. T.; Sunaryono, S. Fe₃O₄-graphene/polyethylene glycol-SiO₂ as a phase change material for thermal energy storage. *Mater. Chem. Phys.* **2023**, *310*, No. 128457.
- (35) Liu, S.; Fei, X.; Zhang, B.; Zhao, H.; Wan, M. Expanded graphite/paraffin/silica phase change composites with high thermal conductivity and low permeability prepared by the solid-state wet grinding method. *Sol. Energy Mater. Sol. Cells* **2022**, *236*, No. 111484.
- (36) Raulo, A.; Suin, S.; Paria, S.; Khatua, B. B. Expanded graphite (EG) as a potential filler in the reduction of percolation threshold of multiwall carbon nanotubes (MWCNT) in the PMMA/HDPE/EG/MWCNT nanocomposites. *Polym. Compos.* **2016**, *37* (7), 2070–2082.
- (37) Nguyen, G. T. Polyethylene glycol/fumed silica composites as shape-stabilized phase change materials with effective thermal energy storage. *RSC Adv.* **2023**, *13* (11), 7621–7631.